Evaluation of a limit equilibrium model to simulate crush pillar behaviour

by M. Du Plessis*, D.F. Malan†, and J.A.L. Napier†

Synopsis

This paper describes the evaluation of a limit equilibrium model to simulate the behaviour of crush pillars in platinum mines. An analytical model was derived to calculate the residual average pillar stress (APS) values of the crush pillars. The values predicted by this model were compared to the numerical values obtained from TEXAN simulations. In general, the limit equilibrium model appears to be very attractive for simulating pillar failure as the gradual crushing of the outside of the pillar and the transfer of stress to the intact core can be replicated. The value of the TEXAN crush pillar model was further demonstrated by simulating an idealized layout with crush pillars between two adjacent panels. The simulations illustrated that oversized pillars will not crush close to the face and this may lead to seismic failure in the back area. An important finding of the study is that closure measurements may prove to be a very valuable diagnostic measure in crush pillars layouts. Distinct differences in magnitudes of closure were simulated for a scenario where the pillars crush as expected, compared to the scenario where an oversized pillar is left. Experimental closure data collected in a crush pillar stope provided further evidence regarding the value of closure measurements in these layouts.

Keywords
mine design, crush pillars, numerical analysis, limit equilibrium model.

Overview of crush pillars

Crush pillars are commonly used in the intermediate-depth platinum mines. These pillars are designed to be crushed in the face and allow for higher extraction ratios, as this prevents 'back breaks' and generally leads to stable conditions[1]. Rustenburg Platinum Mine (Rustenburg Section) was the first platinum group to implement the use of crush pillars as early as 1974[2]. The design of crush pillar layouts was initially conducted using pillar dimensions that were successful in other areas. The pillar dimensions and spacings were then adjusted until the pillars provided the required behaviour[2]. The typical range of width/height (w/h) ratios of the crush pillars varied between 1.5–2.5. This accommodated the varying stoping widths (0.9 m–2 m), the weak footwall rock in some areas, and structural weaknesses in the rock. An alternative design approach was to cut the pillar at a w/h ratio of 2 and then increase or decrease the pillar width until crushing was achieved.

Ozbay *et al.*[2] state that the main purpose of the crush pillars is to provide enough resistance to support the rock up to the highest known parting plane (i.e. Merensky Bastard reef contact at a height of 5 m–45 m) and not to support the full overburden rock mass to surface. A typical mining configuration for a crush pillar layout consists of pillars being positioned either adjacent to raises/winzes (dip mining) or strike gullies (breast mining). The pillars are separated in the direction of mining by a holing to allow for either ventilation (vent holing) or to increase extraction (pillar holing). Crush pillar layouts typically consist of approximately 30 m–33 m wide panel spans (inter-pillar) with slender pillars 2 m, 2.5 m, 3 m, or 4 m wide and 3 m, 4 m, or 6 m in length. The pillars are separated by 0.5 m to 3 m wide holings. A siding is mined adjacent to the raise or gully to ensure that the failed pillar material does not fall into the travelling way. Figure 1 shows a photograph of a crush pillar. Figure 2 is an example of a typical up-dip crush pillar layout. An off-reef haulage provides a link to the reef horizon via a cross-cut and a travelling way.

In most mining operations, the design of the crush pillars is based on trial and error. As the pillar strength is unknown, the pillar sizes are adjusted to obtain the desired behaviour. Several factors affect the behaviour of the crush pillars and in many cases satisfactory pillar crushing is not achieved. This results in a seismic hazard in many of the mines using

* *Lonmin Platinum, South Africa.*
† *Department of Mining Engineering, University of Pretoria.*

 SA ISSN 0038–223X/3.00 + 0.00. Paper received Aug. 2011; revised paper received Sep. 2011.

Evaluation of a limit equilibrium model to simulate crush pillar behaviour

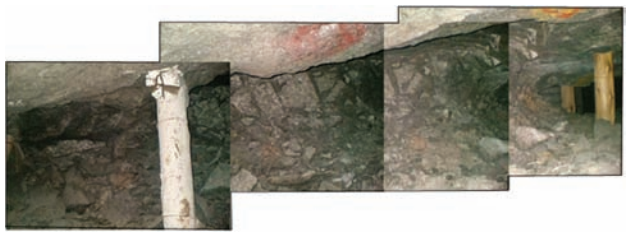

Figure 1—Photograph of a crush pillar (after Canbulat *et al.*[3])

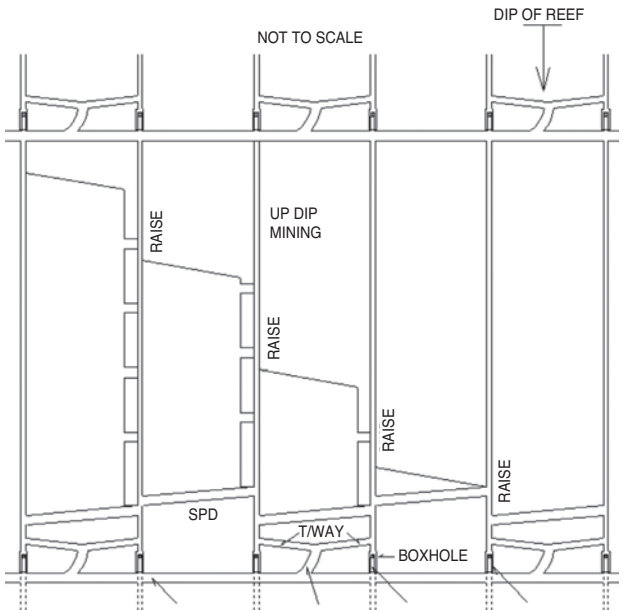

Figure 2–Typical layout (up-dip mining) for a narrow tabular reef mine using crush pillars (after Jager and Ryder[1])

crush pillars, as larger pillars may burst. Some of the factors affecting crush pillar behaviour are:

- Stope layouts, which include the position of the pillars, the presence of a siding, the stoping width, the panel span, and the pillar size
- Rock mass 'stiffness' and the influence of regional pillars
- Strength of the pillar foundation relative to the pillar strength and load being applied
- Peak and residual pillar strength.

During the past four decades, several of these parameters were studied in an attempt to better understand and predict the behaviour of the pillars (see, for example the references in Watson *et al.*[4]). Crush pillar layouts have, however, remained essentially unchanged over this period. The objective of this paper is to evaluate a limit equilibrium model to simulate the behaviour of these pillars. This will allow the behavior of these pillars to be simulated in displacement discontinuity boundary element programs such as TEXAN. Numerical modelling studies can then be used to investigate some of the factors described above.

Typical crush pillar behaviour

The measured and observed behaviour of a 2:1 Merensky crush pillar is summarized in Figure 3 and Table I. Based on stress measurements, Roberts *et al.*[5] determined that a crush pillar reaches its peak strength at between 3–10 millistrains, then fails following a further compression of approximately 5 millistrains along an estimated negative post-peak stiffness slope of 12 GN/m. Following further compression of the order of 50–90 millistrains, it is assumed that footwall heave occurs as a result of the lateral confinement of the foundation. At this point it is assumed that the crushing of the foundation restricts the load capacity of the pillar as the pillar is reliant on the foundations, which is believed to be the limiting load-bearing component. Further compression could result in an increase in the contact friction angle; the result is a 'squat effect', with the slope of the stress strain curve becoming positive. This is assumed to occur when the vertical strain is > 0.4.

Of significance is the high residual crush pillar strength of 13–25 MPa (Table I). The fact that failed pillars with a relatively small width to height ratio (2:1) do maintain such a large residual strength is not always appreciated. The function of crush pillars is to support the tensile zone between regional support or to provide support up to any well-defined partings in the hangingwall. Pillars would not have been able to fulfill this function if they did not maintain these large residual strength values.

The value of the peak pillar strength is unknown. The values quoted in Table I are based on estimates as described by Ryder and Ozbay[6].

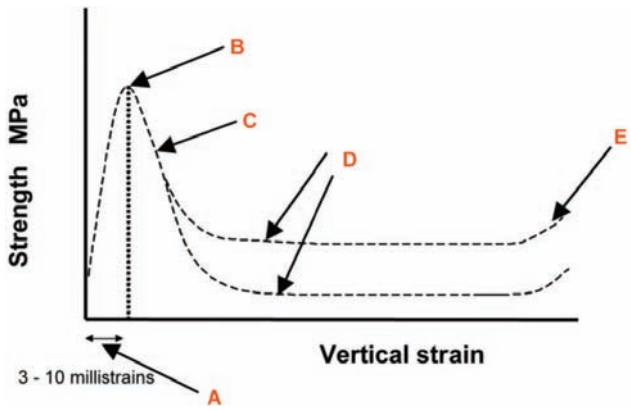

Figure 3—The stress-strain curve of a 2:1 crush pillar (after Roberts *et al.*[5])

Table I

Estimated behaviour of a crush pillar with a w:h ratio of 2:1 (after Roberts *et al.*[5])

Position	Behaviour	Value	Unit
A	Stope closure	(3–10)	Millistrains
B	Peak strength	75–150	MPa
C	Post failure slope	12	GN / m
D	Residual pillar strength	13–25	MPa
E	Squat effect	50–90	Millistrains

Evaluation of a limit equilibrium model to simulate crush pillar behaviour

A recent study on crush pillar behaviour published by Watson *et al.*[4] indicates that the following three factors need to be considered for the design of a crush pillar.

1. Residual strength requirements
2. Loading stiffness of the environment, and how this varies with distance from the face
3. The relationship between peak pillar strength and w/h ratio.

The focus of the study was only on Merensky crush pillars, and design charts were developed by Watson *et al.*[4] for these pillars. The relationship between residual pillar strength and w/h ratio was determined by underground stress measurements. It was found that no further strength increase occurred above a w/h ratio of about three (Figure 4). However, limited laboratory tests, in which an attempt was made to reproduce punching, showed an exponential increase up to a w/h ratio of five (Figure 5). This exponential increase in residual strength with w/h ratio was also shown by analytical solutions used by the authors.

A limit equilibrium model to simulate crush pillar behaviour

A major challenge in the design of pillar layouts is to integrate an appropriate representation of the pillar failure behaviour with the overall analysis of the interactive tabular mining stress distribution. This is computationally demanding. The detailed inelastic analysis of seam or reef crushing behaviour is most appropriately conducted by means of nonlinear finite element or finite difference models, whereas the tabular excavation layout stress interactions in three dimensions can be efficiently represented using a boundary element model based on classical displacement discontinuity elements. Some simplification of the problem is possible if the fractured seam or reef material is known to be concentrated within or close to the mining horizon and does not extend appreciably into the hangingwall or footwall regions. This will often be the case when considering the design of crush pillars in shallow pillar mining layouts. Various strategies have been suggested to represent nonlinear seam behaviour using limit equilibrium methods (for example, Brummer[7]) or the so-called 'enhanced' displacement discontinuity method (Yacoub and Curran[8]), in which reef-parallel strain components are included in the set of unknown variables that are evaluated on the reef horizon. In the present study an analytic limit equilibrium model, similar to coal seam deformation models introduced by Barron[9], is employed to represent the behaviour of the reef material in pillars. Napier and Malan[10] carried out a preliminary evaluation of a similar model and demonstrated that it is feasible to model pillar crushing and burst instability effects. The objective of this paper is to extend this original evaluation of the model. It should be noted that Salamon[11] introduced a refinement of this model which he called the 'enhanced confined core concept' of pillar strength. The focus of the work for this current paper was nevertheless restricted to the simpler model as defined below to illustrate the value of these limit equilibrium models when implemented in boundary element codes such as TEXAN[10, 12].

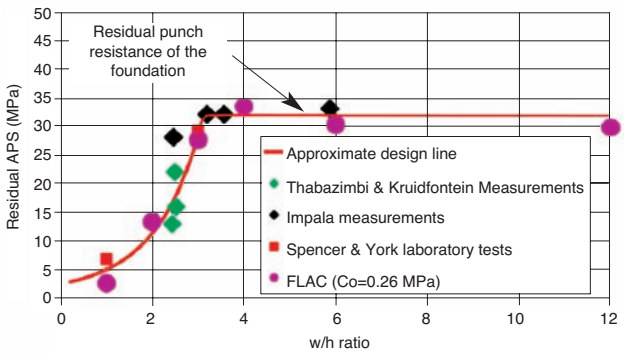

Figure 4—Pillar residual strength as a function of w/h ratio (after Watson *et al.*[4])

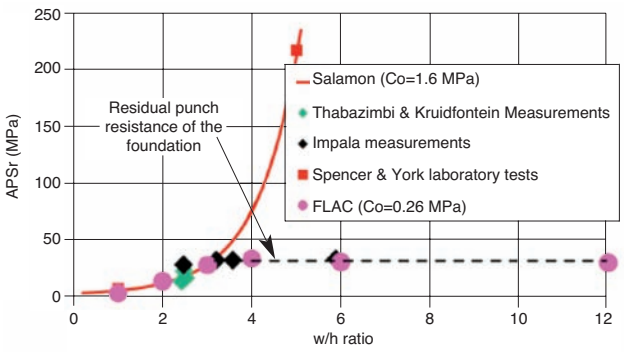

Figure 5—Pillar w/h ratio strengthening effects on residual APS (after Watson *et al.*[4])

Formulation of the model

The force equilibrium of a material 'slice' of a pillar is shown in Figure 6.

It is assumed that the edge of the pillar is at $x = 0$ and that the seam-parallel stress component σ_s is uniform over the height of the pillar and increases as x increases. From Figure 6 it can be inferred that the equilibrium force balance acting on the slice of height H and unit out of plane width requires that:

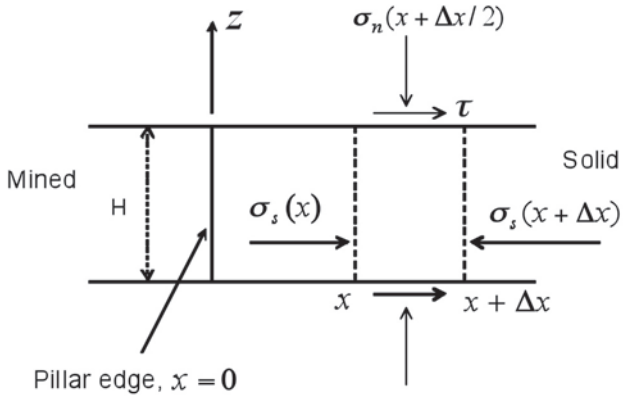

Figure 6—Force equilibrium of elementary material slice between two bounding surfaces

$$H\sigma_s(x+\Delta x) = H\sigma_s(x) + 2\tau\Delta x \quad [1]$$

Taking the limit $\Delta x \rightarrow 0$ Equation [1] can be written in the form of the differential equation;

$$\frac{d\sigma_s}{dx} = 2\tau / H \quad [2]$$

Equation [2] can be solved for σ_s if a relationship exists between τ and σ_s. This can be established by making the following assumptions:

(a) Assume that τ is related to the surface-normal stress σ_n by a frictional slip condition of the form:

$$\tau = \mu\sigma_n \quad [3]$$

where μ is the friction coefficient.

(b) Assume that σ_n is related to the average stress σ_s by a failure relationship of the form:

$$\sigma_n = S + m\sigma_s \quad [4]$$

where S and m are specified constants.

Substituting Equations [4] and [3] into Equation [2] yields the required differential equation as follows:

$$\frac{d\sigma_s}{dx} = \frac{2\mu}{H}(S + m\sigma_s) \quad [5]$$

Equation [5] can be integrated directly if it is written in the separable form

$$\int \frac{d\sigma_s}{S + m\sigma_s} = \int \frac{2\mu}{H} dx \quad [6]$$

Integrating Equation [6] yields the solution to Equation [5] in the form

$$\ln(S + m\sigma_s) = \frac{2\mu m x}{H} + A \quad [7]$$

where A is a constant that can be determined by applying the boundary condition that the average horizontal stress σ_s is equal to an edge constraint stress p when $x = 0$. Hence, substituting $\sigma_s = p$ and $x = 0$ in Equation [7] yields $A = \ln(S + mp)$. The average horizontal stress is then recovered from Equation [7] as a function of the distance x from the edge of the pillar in the form

$$\sigma_s = (S/m + p)\exp(2\mu m x / H) - S/m \quad [8]$$

The seam-normal stress component σ_n can be obtained by substituting the expression for σ_s given by Equation [8] into Equation [4] to yield

$$\sigma_n = (S + mp)\exp(2\mu m x / H) \quad [9]$$

It is apparent from an examination of Equations [8] and [9] that the solutions for σ_s and σ_n become degenerate (have zero values) if both S and p are equal to zero. In order to proceed further with the application of the simple limit equilibrium model some explicit assumption has to be made concerning the choice of suitable values for S and p. In the present paper, it is assumed $p = 0$ and that the average unconfined strength of the material at the edge of the pillar in the failed state is equal to S. This assumption is tenable if the pillar is able to bear some vertical load at the unsupported edge $x = 0$. Specifically, from Equation [9], the vertical load is $\sigma_n = S$ when $x = 0$. If the pillar edge is, in fact, free-standing then this must be the case. However, it is apparent that the depth of the failed edge zone will be very sensitive to the exact choice of S. While it is not obvious what controls this parameter in actual crush pillars, it is essential that it be carefully calibrated in order to obtain realistic modelling results.

Setting $p = 0$ in Equations [8] and [9] and defining $\alpha = 2\ \mu m/H$ yields the following expressions for the average horizontal and vertical stress values in the edge region:

$$\sigma_s = S(e^{\alpha x} - 1)/m \quad [10]$$

$$\sigma_n = Se^{\alpha x} \quad [11]$$

It is worth noting the differences between the simple average stress model depicted in Figure 6 and an extended limit equilibrium model that has been presented by Salamon[11], which allows for an explicit variation of the stress components σ_{xx}, σ_{zz} and σ_{xz} as functions of both the edge distance coordinate x and the vertical coordinate position z between the floor and roof of the pillar region. Salamon[11] assumes that the material satisfies a limit equilibrium relationship between the maximum and minimum local principal stress components σ_1 and σ_3 at each point (x,z) in the failed region that is of the form

$$\sigma_1(x,z) = m\sigma_3(x,z) \quad [12]$$

The values of the principal stress components σ_1 and σ_3 can be expressed as functions of the individual stress components σ_{xx}, σ_{zz}, and σ_{xz} which are in turn defined in terms of the derivatives of an Airy stress function, $\Phi(x,z)$ that is assumed to have the form

$$\Phi(x,s) = \exp[ax + f(z)] \quad [13]$$

Substituting these expressions into Equation [12] allows the stress components to be solved in a closed but rather complicated form[11]. From the assumed relationship (12), it is noted that this model assumes that the cohesive strength, $S = 0$, and requires the specification of a non-zero confining stress, p, at the edge of the pillar. No allowance is made for roof or floor foundation failure processes and all stress components increase exponentially from the pillar edge. Salamon's model is incomplete in the sense that no general prescription is given for determining the shape of the interface surface between the material in limit equilibrium and the intact material in the interior of the pillar. Initial studies are directed therefore towards evaluating the simple average stress model expressed by Equations [10] and [11].

As pointed out by Salamon *et al.*[13], a Mohr-Coulomb plasticity model without strain softening behaviour is inadequate for simulating actual pillar behaviour where rapid load shedding or 'bursting' may occur. In order to allow for this behaviour, it is assumed that initial failure in the seam or reef material is controlled by an additional constraint relationship of the form

$$\sigma_n \leq S_0 + m_0\sigma_s \quad [14]$$

where S_0 and m_0 represent the intact strength of the pillar material. The constraint expressed by Equation [14] is also used to determine the boundaries between the intact core region of the pillar and the failed edge regions where Equations [10] and [11] are obeyed.

Evaluation of a limit equilibrium model to simulate crush pillar behaviour

Analytical solution for the APS of a failed 2D pillar

Equation [11] predicts an exponential increase in the pillar stress away from the edge towards the centre of the pillar. If the pillar width is w and if the pillar is completely failed then, assuming that the stress profile is symmetric about the centre of the pillar, the average stress in the pillar is given by:

$$APS = \frac{2\int_0^{\frac{w}{2}} \sigma_n dx}{w} \quad [15]$$

By substituting Equation [11] into [15], it follows that:

$$APS = \frac{2S\int_0^{\frac{w}{2}} e^{ax} dx}{w} = \frac{2S}{\alpha w}\left[e^{\alpha w/2} - 1\right] \quad [16]$$

Substituting $\alpha = 2\ \mu m/H$ into Equation [16], the average pillar stress can be expressed as

$$APS = \frac{SH}{\mu m w}\left[e^{\frac{\mu m w}{H}} - 1\right] \quad [17]$$

The form of Equation [17] suggests that the average stress can be written compactly in the following dimensionless form

$$\frac{APS}{S} = \frac{e^{\beta} - 1}{\beta} \quad [18]$$

where the constant $\beta = \mu m w/H$ represents a non-dimensional parameter that is proportional to the width to height ratio. In the limiting case when the width w becomes very small, $\beta = \rightarrow 0$ and $APS \rightarrow S$. This clearly indicates that some caution should be exercised in using the simple limit equilibrium model for very slender failed pillars where $w < H$.

The behaviour of the model derived above can be illustrated using a specific choice of the basic parameters. The following constants were assumed for the initial comparison: $S = 5$ MPa, $m = 2$, $\mu = \tan\phi = \tan 30°$, $w = 10$ m, and $H = 5$ m. If these values are inserted into Equation [17], it is found that the APS = 19.63 MPa. This value was compared with the numerical modelling example described below.

It should be noted that the residual APS value for a failed pillar predicted by Equation [17] is very sensitive to the width to height ratio of the pillar. To illustrate this, Equation [17] is plotted for different width to height ratios (Figure 7). The other parameters used were $S = 5$ MPa, $m = 2$ and $\mu = \tan\phi = \tan 30°$.

To illustrate the effect of different friction angles, Equation [17] is plotted for friction angles from 5° to 45° (Figure 8). The other parameters used were $S = 5$ MPa, $m = 2$ and $w = 10$ m and $H = 5$ m. Note that as the friction angle approaches zero, the residual APS tends to S.

Implementation of the crush pillar model in TEXAN

An overview of the TEXAN tabular excavation computer program is given in Napier and Malan[12]. The code can currently solve both two-dimensional and three-dimensional problems with multiple interacting tabular reef planes and planar fault planes. These planes are tessellated with displacement discontinuity elements to represent stope ride and elastic convergence movements or to model slip movements on fault planes. Elements can be in an 'infinite' space or in a 'semi-infinite' space with a flat, stress-free surface. The medium is assumed to be elastic and isotropic. Analytical kernel expressions are used to compute half-space influence functions in three-dimensions. Elements can be two-dimensional line segments, three-dimensional triangles or three-dimensional convex quadrilaterals. (In particular, square elements can be used if required). Both in-plane and anti-plane components are allowed in two-dimensional analyses.

Each element can have one or more internal collocation points giving constant or higher-order variation discontinuity densities. Triangular elements can be defined to have 1, 10, or 15 internal collocation points giving constant, cubic (third order), or quartic (fourth order) discontinuity variations respectively. Quadrilateral elements can be defined with 1 or 9 internal collocation points. A quadrilateral element with 9 internal collocation points is assigned a bi-quadratic shape function (degenerate fourth order).

Stress and displacement field values (so-called 'benchmark' values) close to excavation surfaces are accurately computed with higher-order elements if the normal projection of the field point falls within the element perimeter. Stress singularities can nevertheless arise close to element boundaries (approximately within 0.1 of the element 'diameter'). Field values cannot be computed accurately within a distance of approximately two to three element 'diameters' normal to the element plane when using constant elements.

Additional attributes of the TEXAN code include the ability to specify mixed displacement and stress component boundary conditions on specific elements, the inclusion of

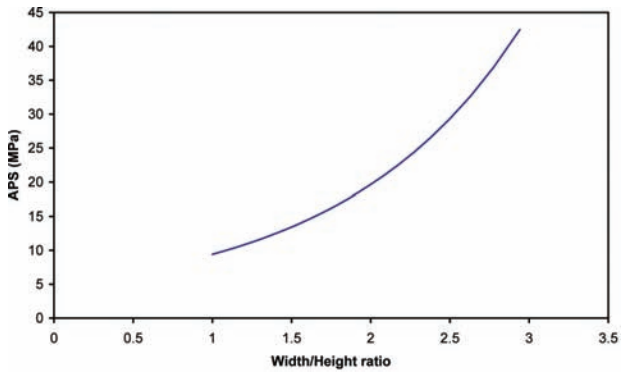

Figure 7—Simulated residual APS values for a failed pillar at different width to height ratios

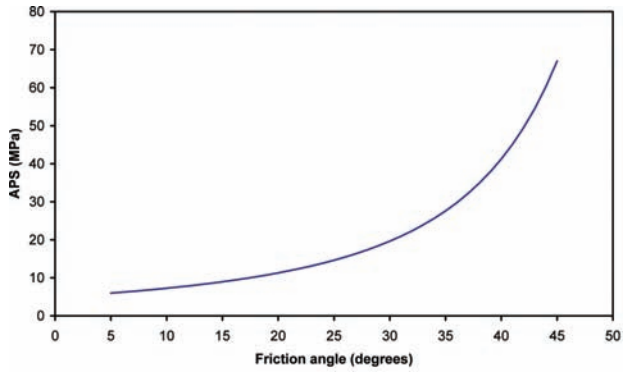

Figure 8—Simulated residual APS values for a failed pillar as a function of assumed friction angle

backfill regions in mined areas, and the ability to simulate fault slip processes by activating pre-defined element tessellations in sequential mining steps.

Regarding the limit equilibrium model, the examples given in the previous section are relevant to plane strain layout configurations and, therefore, are of limited use in tabular layout pillar design. It will be very difficult to extend the simple differential relationship embodied in Equation [5] to the case of a pillar having an irregular, two-dimensional plan shape. In particular, it is apparent that the slip field orientation in the pillar should depend on the relative magnitude and direction of the in-seam principal stress components and the detailed pillar shape. In order to maintain the appealing features of the simple model, it is assumed that Equations [10] and [11] can still be applied at each internal pillar element collocation point where stress conditions are evaluated. The crucial assumption is made that the distance that is used at each such point is interpreted as the closest distance from the point to the relevant polygonal edge defining the pillar shape. It is straightforward to compute this distance for all pillar and abutment element collocation points. This simple strategy then permits the limit equilibrium model to be extended to general tabular layout problems with irregularly shaped pillars.

Numerical modelling of the APS of a failed pillar

A specific model geometry simulated with the TEXAN code is shown in Figure 9. It was attempted to simulate a 'rib' pillar to approximate the two-dimensional solution of APS given above. The pillar was simulated at a depth of a 1000 m and the stress gradient was 0.031 MPa/m.

Figure 10 illustrates the stress distribution along Section AA' for the rigid pillar. Note the classical stress profile for a simulation in which the pillars are assumed to be rigid (incompressible).

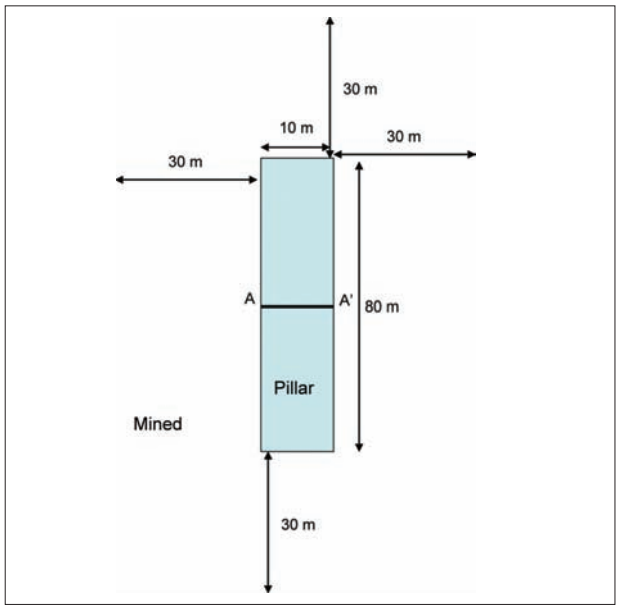

Figure 9—Layout simulated. Square elements of 1 m size were used for the initial simulation. The stress profile along section AA' was plotted. The pillar was simulated as a rigid pillar and then allowed to crush in a second simulation

The simulated APS value for the pillar (average of all 800 collation points) was 110.56 MPa. In comparison, Figure 11 illustrates the stress profile along section AA' if a limit equilibrium model is assumed and the parameters given previously are assumed (S = 5 MPa, m = 2, $\mu = \tan\phi = \tan 30°$, and H = 5 m; the peak and residual values are assumed to be similar). The behaviour predicted by Equation [11] is also plotted in the figure.

The average of the 10 simulated values across section AA' is 19.48 MPa. This is in close agreement with the analytical value of 19.63 MPa calculated using Equation [17]. The average APS for the entire pillar is 18.65 MPa. This is slightly lower owing to the effects at the two ends of the pillar (an infinite long rib pillar was only approximated but not simulated).

From Figure 11, a key attribute of the limit equilibrium model is clearly visible: The stresses increase in an exponential fashion towards the centre of the pillar. Salamon[11] identified this as a potential problem as it may lead to the formation of unduly high stresses in the core of wide pillars. The magnitude of these stresses may become sufficiently high to cause failure in the hangingwall or footwall. The current model as implemented in TEXAN can allow this off-reef failure to be evaluated in restricted cases by allowing shear failure planes to grow from the pillar edges.

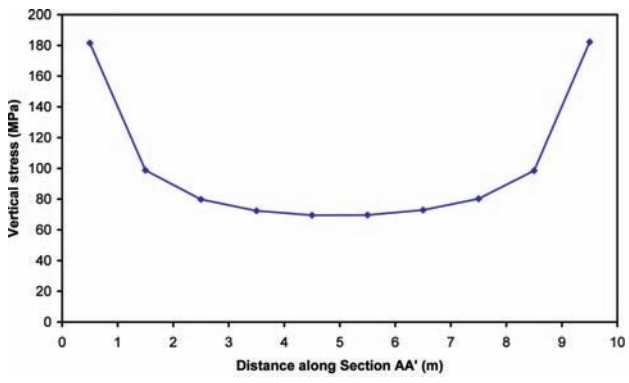

Figure 10—Simulated vertical stress along section AA' for a rigid pillar

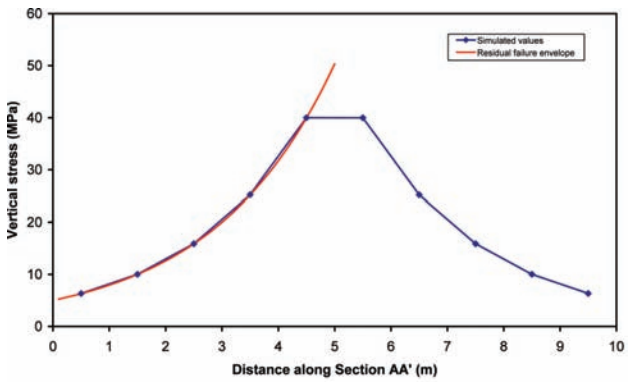

Figure 11—Simulated vertical stress along section AA' for a limit equilibrium model

Evaluation of a limit equilibrium model to simulate crush pillar behaviour

Effect of element size

Regarding APS calculations using displacement discontinuity boundary element programs, Napier and Malan[14] have illustrated that the simulated APS can depend on the chosen mesh size. Regarding the limit equilibrium model, it is expected that the mesh size will also play a role. This is of particular importance when simulating a large-scale crush pillar layout as the pillar width may be as small as 2–3 m. In TEXAN, the limit equilibrium equation is applied at each internal pillar point where stress conditions are evaluated. The distance that is used at each such point is interpreted as the closest distance from the point to the relevant polygonal edge defining the pillar shape. This closest distance will be dependent on the element tessellation covering the pillar, and care should be taken that the average element size is much smaller than the width of the pillar. To investigate this effect, the geometry shown in Figure 9 was simulated using the same modelling parameters but with different element sizes. Figure 12 illustrates the effect of element size when using square constant-strength (single collocation point) elements. As expected, very coarse element sizes (5 m) will underestimate the residual strength of the failed pillar. The few element collocation points present fall outside the higher stresses of the central core of the failed pillar and therefore underestimate the average stress. Note that the data point for the 2 m element size is considered as an 'outlier' as this is the only size where an uneven number of elements were required to cover the width of the 10 m pillar. This resulted in the collocation point of the centre row of elements capturing the high stress value in the centre of the pillar (see Figure 11).

The effect of using an irregular mesh of triangular elements was also investigated. An example of such a mesh covering the pillar is shown in Figure 13. Simulations with various average element sizes were conducted. The results are shown in Figure 14. Of interest is that the residual APS is much less sensitive to mesh size than for the regular mesh consisting of square elements.

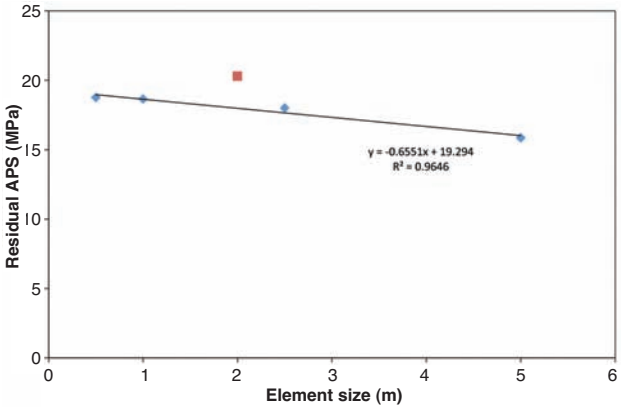

Figure 12—Effect of element size (square single collocation point elements) on simulated residual APS of a 10 m wide pillar (Figure 9). The 2 m element size (red square) was excluded from the trend line calculation (see discussion in text)

Simulation of crush pillar behaviour

The examples presented above illustrate the potential utility of the simple limit equilibrium model to simulate the behaviour of crush pillars. When such a model is implemented in a suitable boundary element code, it will allow for the simulation of large-scale platinum mine layouts utilizing these pillars. The effect of parameters such as depth, potholes, regional pillars, and oversized pillars on the crushing of the pillars can now be investigated. As an illustration of this capability, the TEXAN code was used to simulate an idealized crush pillar layout. The simulated layout is shown in Figure 15. It consists of a 30 m x 70 m stope panel with a second panel being mined in a sequential fashion adjacent to this first panel. The layout was simulated using eight mining steps with seven crush pillars being formed in this process. For the second panel, the size of each mining step was 10 m and the sizes of the crush pillars were 4 m x 6 m (w:h = 2). These dimensions may not necessarily be realistic when compared to actual layouts, but were assumed in order to illustrate the behavior of the crush pillar model.

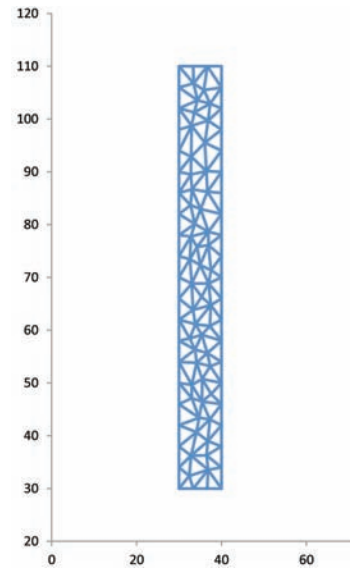

Figure 13—Example of the tessellation of triangular elements used for the pillar shown in Figure 9

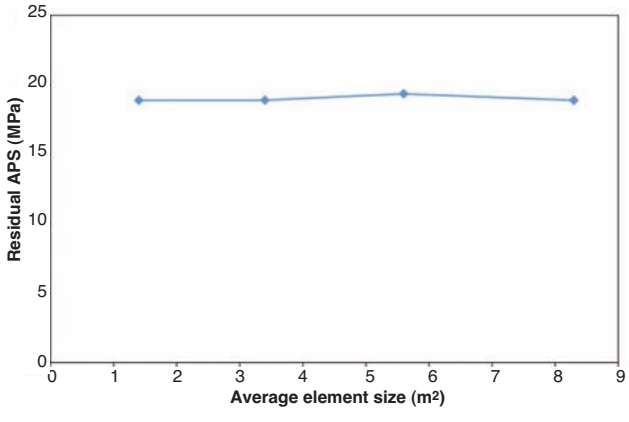

Figure 14—Effect of element size (triangular single collocation point elements) on the simulated residual APS of a 10 m wide pillar (Figure 9)

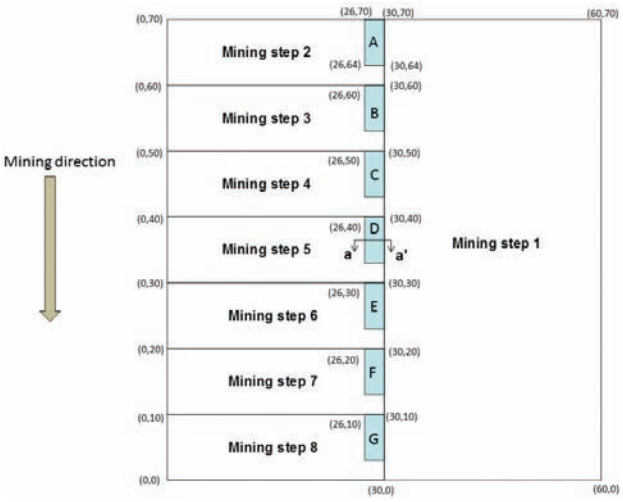

Figure 15—Idealized crush pillar layout simulated in the TEXAN code

Table II

Parameters used for the crush pillar simulation

General parameters	Value
Young's modules	70 GPa
Poisson's ratio	0.25
Stress gradient	0.03 MPa/m
Depth	600 m
Reef dip	0°
Crush model parameters	**Value**
Intact cohesion C_0	5 MPa
Residual cohesion C	5 MPa
Intact slope m_0	5
Residual slope m	3
Bounding friction angle	35°
Seam height	2 m
Seam stiffness modulus	10^6 MPa/m

The parameters used for the simulations are shown in Table II. Note that these values were chosen arbitrarily and that a better calibration of this model based on underground measurements will be required in future.

For the first simulation, the pillars were not allowed to crush and were simulated as 'rigid' pillars in an elastic rock mass. Figure 16 illustrates the expected increase in pillar stress as the pillars move into the back area. The run was repeated using the crush pillar model, and Figure 17 illustrates the APS values on three of the pillars (D,E, and F) as a function of mining step. Note that the pillar stress gradually increases as the mining faces approach. For the chosen parameters, the peak APS value is achieved during the mining step when the pillars are formed. The pillar then crushes completely during the next mining step and the residual APS is maintained thereafter. For the crush pillar model, the peak stress on the pillars (≈ 56 MPa) is far less than for the pillars that are not allowed to fail (≈ 130 MPa).

Figure 18 illustrates the stress profile along section aa' (Figure 15) for pillar D. After step 1, the pillar is still part of the abutment of the first panel. It can be seen from the stress profile that some crushing of this abutment has already occurred and the peak stress value is located approximately 1.25 m inside the rock. This stress peak gradually moves deeper into the rock as can be seen for the profile of step 4. During step 5 the pillar is formed and the profile becomes nearly symmetrical. During the next step, the stress increase causes complete failure of the core and the residual stress profile is assumed.

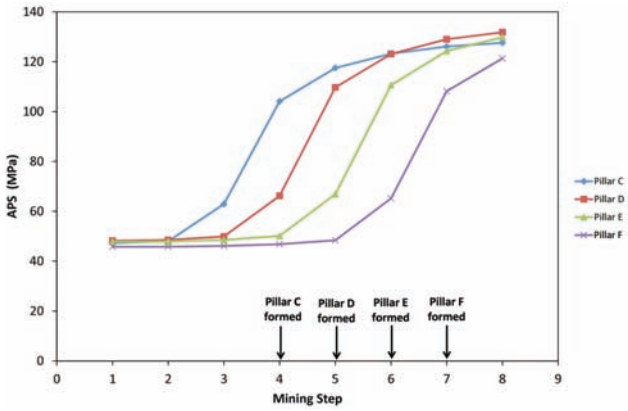

Figure 16—Simulated pillar stress if the pillars are not allowed to crush ('rigid' pillars)

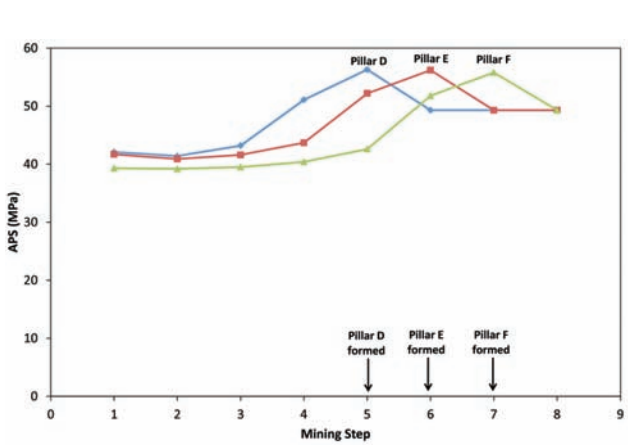

Figure 17—Simulated pillar stress if the pillars are allowed to crush (limit equilibrium model)

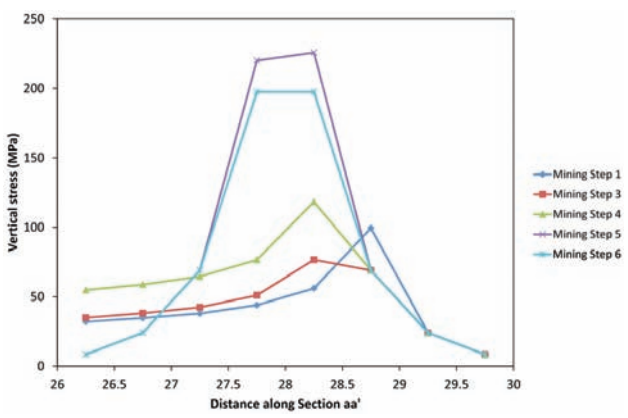

Figure 18—Simulated stress profile for pillar D along section aa' (see Figure 15) for the different mining steps

Evaluation of a limit equilibrium model to simulate crush pillar behaviour

Effect of oversized pillars

A problem endemic to crush pillar layouts is the poor cutting of the pillars, and this frequently results in oversized pillars being present in these layouts. The larger pillars do not always crush in a stable manner and may fail violently in the back areas. The idealized crush pillar layout simulated above was used to investigate the effect of an oversized crush pillar. The geometry simulated was identical to that shown in Figure 15 except that pillar D was increased in size to a 6 m x 6 m pillar (w:h = 3). The modified geometry is shown in Figure 19.

The simulated stress values for pillar D (6 m x 6 m) are shown in Figure 20 and compared to the smaller pillar (4 m x 6 m) of the first simulation. Note that the APS value of the larger pillar is 73 MPa after step 8. This is much larger than the 49 MPa simulated for the 4 m x 6 m pillar. Figure 21 illustrates the stress profile along section bb' (see Figure 19) for pillar D. Note that the core of the pillar is still intact and this may lead to violent failure in the back area if the pillar becomes more highly stressed. As part of future studies, it is planned to investigate the failure of these oversized pillars in the back areas of stopes after more mining steps have occurred. Some preliminary work regarding possible 'pillar bursting' after a number of mining steps has already been described in Malan and Napier[10].

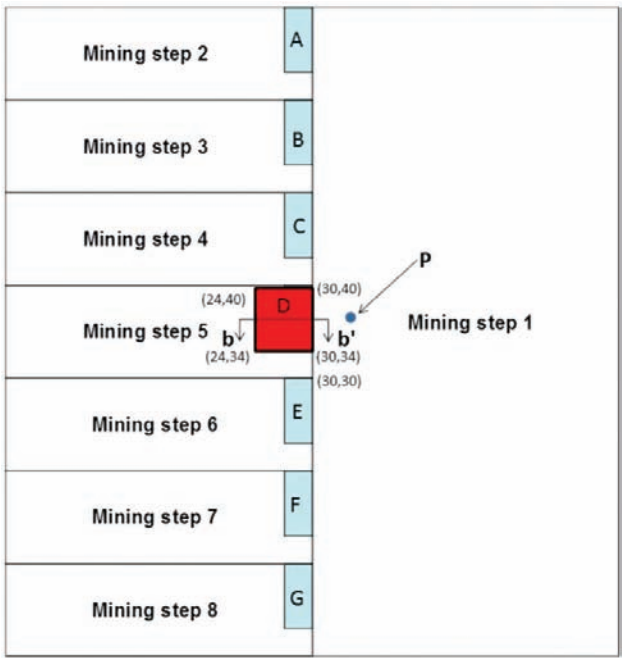

Figure 19—Geometry used to simulate the effect of an oversized crush

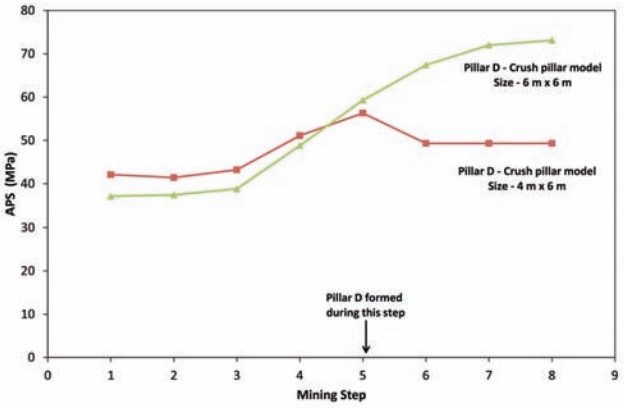

Figure 20—Comparison of the APS value on pillar D for the two pillar sizes. Except for this difference in size, all other model parameters were identical. Note that the 6 m x 6 m pillar does not crush to the same extent as the 4 m x 6 m pillar

Stope closure as a diagnostic tool in crush pillar layouts

Currently there is no simple method to determine whether crush pillars are behaving according to expectations. For rock engineers, it is important to determine whether these pillars are fully crushed close to the face or not. Some information can be obtained by drilling holes through the pillars and using borehole cameras, but this is tedious and will be difficult to implement on a mine-wide scale. Stress measurements in the core of the pillars will be ideal, but this is not practical owing to the high cost involved and the difficulties with rock stress measurements in general. An alternative option may be to monitor stope closure, as there appears to be distinct differences in closure behaviour between panels using stable pillars and those using correctly designed crush pillars. To illustrate this behaviour, the closure at a distance of 5 m from pillar D in the first mining panel (point P in Figure 19) is plotted in Figure 22. It is clear that a noticeable increase in closure is observed if the pillars are allowed to crush compared to a stable pillar layout. Also of interest is that the oversized pillar in Figure 19 led to a reduction in closure behavior compared to a pillar that crushes normally in this area.

Experimental stope closure in a crush pillar layout

Experimental data collected by the authors in a crush pillar layout is examined in this section to further investigate the potential of using closure as a diagnostic tool in crush pillar layouts. Down-dip mining was employed at the experimental site on the Merensky Reef (Figure 23). The mining configuration left behind 3.5 m x 2 m crush pillars along dip. Some of these pillars did not appear to be crushing completely.

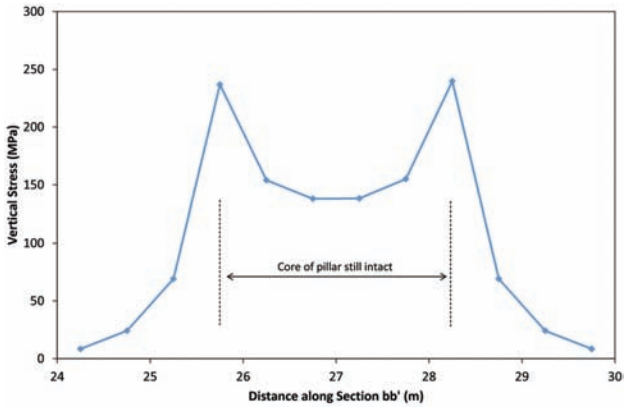

Figure 21—Stress profile along section bb' (Figure 19) for the oversized pillar D after mining step 8

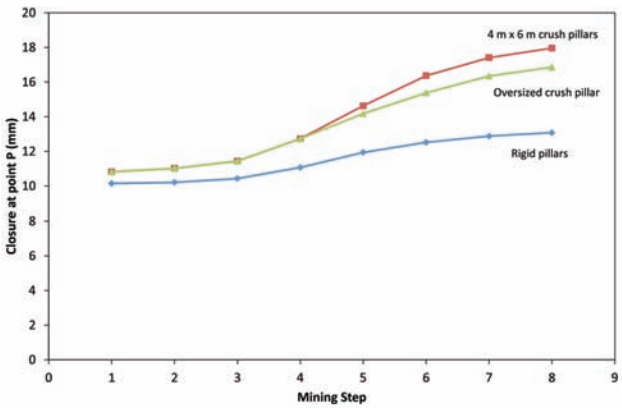

Figure 22—Simulated increase in closure at point P (see Figure 19) as a function of mining step

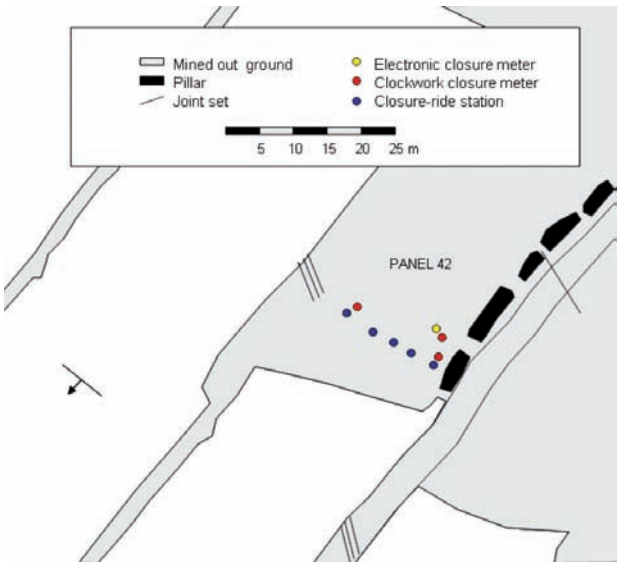

Figure 23—Plan showing the extent of mining in the immediate vicinity of an experimental area where the behaviour of the crush pillars was examined. The position of the in-panel instrumentation is also indicated

The footwall exposed in the gully to the southeast (downdip side) was a fine-grained grey norite. The Merensky Reef consists of a coarse-grained feldspathic pyroxenite overlain by a medium- to coarse-grained norite, often with euhedral, brown pyroxene grains. It was reported that the Merensky Reef was potholed adjacent to this area, resulting in adverse ground conditions. None of these effects were, however, seen within the experimental panel. In addition, no large-scale structural features, such as dykes or faults, were observed within the panel. The geological contribution to the rock mass behaviour in this vicinity is restricted to joint sets. Figures 24 and 25 are photographs of the experimental panel, showing the rock mass conditions around the closure-ride and closure meters.

The typical closure behaviour in the experimental site is presented below. Data from the closure-ride stations is given in Figure 26. Note that, contrary to measurements in other sites monitored by the authors, the highest rate of closure was not measured in the centre of the panel, but next to the crush pillar. This behaviour is caused by the crushing of the pillar and the presence of a mined panel on the other side of the row of pillars. In this particular case, the closure appears to serve as a useful indicator of the correct pillar behaviour. Oversized pillars would not yield and deform, resulting in lower rates of closure next to the pillar compared to the middle of the panel. At this particular site, the closure also displayed a significant time-dependent component as shown in Figure 27.

It is hypothesized that the time-dependent closure component at the experimental site was caused by the time-dependent crushing of the pillars as they gradually move into the back area. No movement of discontinuities in the hangingwall could be identified that may have contributed to this time-dependent closure. In the absence of blasting, the time-dependent closure gradually decreased with time. If the hypothesis is correct, the stope closure behaviour as monitored during multiple advances may be a useful indicator of stable pillar crushing. A decrease in closure rate

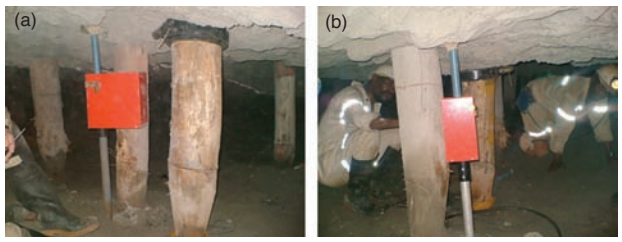

Figure 24—(a) Hangingwall conditions around closure station 1 (closest to pillar) and (b) closure station 2 (centre of panel). In both cases the abundant low-angle discontinuities are dipping towards the face. The low-angle discontinuities terminate against steeper-dipping geological features

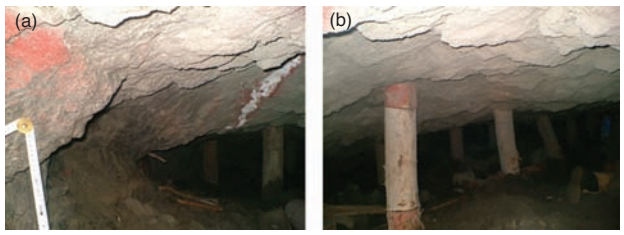

Figure 25—(a) and (b) Views along the sidewall of the crush pillar looking towards the face

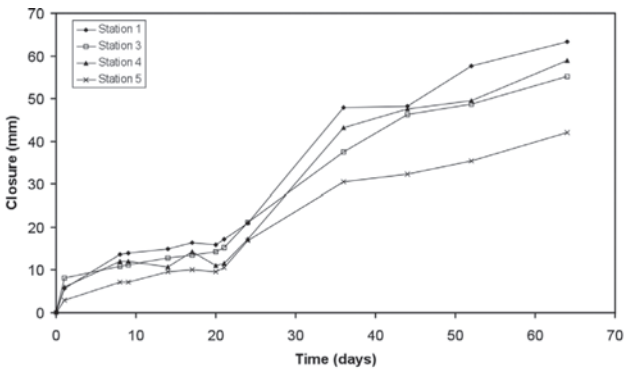

Figure 26—Closure data recorded using the closure-ride stations. Station 1 is next to the crush pillar. A peg of station 2 was lost and the data from this station is therefore not shown on this graph. The rate of closure varied from 0.66 mm/day to 0.98 mm/day

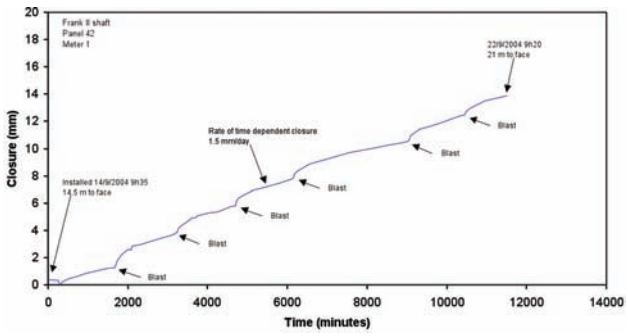

Figure 27—Typical closure recorded by one of the clockwork closure meters (no. 1). Note the presence of a prominent time-dependent closure component

and time-dependent closure may imply that the pillars are oversized and may increase the likelihood of seismicity as they move into the back area. Care should nevertheless be exercised when using absolute closure magnitude as an indicator of pillar crushing, as increasing closure rates may also be associated with unexpected unravelling of the hanging wall.

Neither the limit equilibrium model nor the enhanced model presented by Salamon[11] can replicate the time-dependent closure behavior described above. Further work using the limit equilibrium model will therefore be focused on enhancing the model to include this component. A trial mining site using crush pillars is also being planned at a Lonmin mine, and the limit equilibrium model will be used to guide the planning of this experimental site and the type of monitoring required. Continuous closure measurements and drilling into the pillars to determine the depth of failure will be part of this monitoring programme.

Conclusions

This paper describes the evaluation of a simple limit equilibrium model to simulate the behaviour of crush pillars in platinum mines. The model is currently available as a constitutive code in the TEXAN boundary element program. For the evaluation in this paper, an analytical model was used to calculate the residual APS values of the crush pillars. The values predicted by this model were compared to the numerical values obtained from the TEXAN simulations. Good agreement was obtained between the two models, and this serves as a useful validation of the model implemented in the numerical code. In general, the limit equilibrium model appears to be very attractive for simulating pillar failure, as the gradual crushing of the outside of the pillar and the transfer of stress to the intact core can be replicated.

The value of the TEXAN crush pillar model was further demonstrated by simulating an idealized layout with crush pillars between two adjacent panels. The simulations illustrated that oversized pillars will not crush close to the face and this may lead to seismic failure in the back area.

The study highlighted a key attribute of the limit equilibrium models: the pillar stresses increase in an exponential fashion towards the centre of the pillar. This may lead to the formation of unduly high stresses in the core of wide pillars, and the magnitude of these stresses may become sufficiently high to cause failure in the hangingwall or footwall. The treatment of off-reef foundation failure can be simulated by allowing shear failure surfaces to grow at the edges of designated pillars. This feature of the TEXAN program will be evaluated in future studies.

An important finding of the study is that closure measurements may prove to be a very valuable diagnostic measure in crush pillars layouts. Distinct differences in magnitudes of closure were simulated for a scenario where the pillars crush as expected, compared to the scenario where an oversized pillar is left. Experimental closure data collected in a crush pillar stope provided further evidence regarding the value of closure measurements in these layouts.

As a next step, improved calibration of the limit equilibrium model using underground data from crush pillar sites is required. A trial mining site using crush pillars is also being planned, and the limit equilibrium model will be used to guide the planning of this experimental site and the type of monitoring that is required.

Acknowledgements

This work forms part of the PhD study of Mr M. du Plessis at the University of Pretoria.

References

1. Jager, A.J. and Ryder, J.A. A handbook on rock engineering practice for tabular hard rock mines, *Safety in Mines Research Advisory Committee*, Johannesburg. 1999.
2. Ozbay, M.U., Ryder, J.A., and Jager, A.J. The design of pillar systems as practiced in shallow hard-rock tabular mines in South Africa. *Journal of the Southern African Institute of Mining and Metallurgy*, Jan/Feb, vol. 95, no. 1 1995, pp. 7–18.
3. Canbulat, I., Grodener, N., Lightfoot, N., Ryder, J., Essrich, F., Dlokweni, A., Wilkinson, C., Krog, G., and Pronhaska, G. The determination of loading conditions for crush pillars and the performance of crush pillars under dynamic loading, *Safety in Mines Research Advisory Committee Project* SIM040302. Johannesburg, 2006.
4. Watson, B.P., Kuijpers, J.S., and Stacey, T.R. Design of Merensky Reef crush pillars. *Journal of the Southern African Institute of Mining and Metallurgy*, vol. 110, no. 10, 2010. pp. 581–591.
5. Roberts, D.P., Roberts, M.K.C., Jager, A.J., and Coetzer, S. The determination of the residual strength of hard rock crush pillars with a width to height ratio of 2:1. *Journal of the Southern African Institute of Mining and Metallurgy*, vol. 105, no. 6, 2005. pp. 401–408.
6. Ryder, J.A. and Ozbay, M.U. A methodology for designing pillar layouts for shallow mining. International Symposium on Static and Dynamic Considerations in Rock Engineering, Swaziland, *ISRM*. 1990.
7. Brummer, R.K. Modelling the non-linear behaviour of fractured seams in deep gold mines, APCOM 87. Proceedings of the Twentieth International Symposium on the Applications of Computers and Mathematics in the Mineral Industries. Mining. Johannesburg, The *South African Institute of Mining and Metallurgy*, vol. 1, 1987. pp. 21–32.
8. Yacoub, T.E. and Curran, J.H. Analysis of post-peak pillar behaviour using the enhanced displacement discontinuity method. *Proceedings of the 37th U.S. Rock Mechanics Symposium*, Balkema, 1999. pp. 169–176.
9. Barron, K. An analytical approach to the design of coal pillars. *CIM Bulletin*, vol. 77, no. 868, 1984. pp. 37–44.
10. Malan, D.F. and Napier, J.A.L. Practical application of the TEXAN code to solve pillar design problems in tabular excavations. *SANIRE 2006 Symposium—Facing the Challenges*, Rustenburg, 2006. pp. 55–74.
11. Salamon, M.D.G. Strength and stability of coal pillars. *Workshop on Coal Pillar Mechanics and Design*, US Bureau of the Interior, *US Bureau of Mines*, Santa Fe, USA. 1992.
12. Napier, J.A.L. AND Malan, D.F. The computational analysis of shallow depth tabular mining problems, *Journal of the Southern African Institute of Mining and Metallurgy*, vol. 107, no. 11 2007, pp. 725–742.
13. Salamon, M.D.G., Badr, S., Mendoza, R. and Ozbay, M.U. Pillar failure in deep coal seams: numerical simulation. Proceedings of the 10th Congress of the International Society for Rock Mechanics. *The South African Institute for Mining and Metallurgy*, Johannesburg, 2003. pp. 1011–1018.
14. Napier, J.A.L. and Malan, D.F. Numerical computation of average pillar stress and implications for pillar design, *Journal of the Southern African Institute of Mining and Metallurgy,* vol. 11, no. 12, 2011. pp. ◆